Article

Not peer-reviewed version

Flexible Mechanical Sensors Fabricated with Graphene Oxide-Coated Commercial Silk

Hyun-Seok Jang , Ki Hoon Lee * , Byung Hoon Kim *

Posted Date: 23 May 2024

doi: 10.20944/preprints202405.1547.v1

Keywords: commercial silk; graphene oxide; thermal treatment; pressure sensor; motion sensor

Article

Flexible Mechanical Sensors Fabricated with Graphene Oxide-Coated Commercial Silk

Hyun-Seok Jang [1], Ki Hoon Lee [1,*] and Byung Hoon Kim [1,2,3,*]

[1] Department of Physics, Incheon National University, Incheon 22012, Republic of Korea; slm92jhs@gmail.com
[2] Intelligent Sensor Convergence Research Center, Incheon National University, Incheon 22012, Republic of Korea
[3] Institute of Basic Science, Incheon National University, Incheon 22012, Republic of Korea
* Correspondence: kihoonlee@inu.ac.kr (K.H.L.); kbh37@inu.ac.kr (B.H.K.)

Abstract: Many studies on flexible strain and pressure sensors have been reported due to growing interest in wearable devices for healthcare. However, most are fabricated with multiple ingredients and complicated methods even though commercial textiles, such as cotton, nylon, polyester, and silk were used. Here we present flexible pressure and strain (motion) sensors prepared with only graphene oxide (GO) and commercial silk fabrics and yarns. The pressure sensors were fabricated by simply dipping the silk fabric into GO solution followed by thermal treatment at 400 °C for reduction of GO (rGO). The pressure sensors were made from rGO-coated fabrics, which were stacked in 3-, 5-, and 7-layers. The super-sensitivity of 2.58 $\times 10^3$ kPa^{-1} at low pressure was observed in the 7-layer pressure sensor. The strain sensors were obtained from rGO-coated twisted silk yarns whose gauge factor was 0.307. Although this value is small or comparable to other sensors, it is appropriate for motion sensing. The results of this study show a cost-effective and simple method for the fabrication of pressure and motion sensors with commercial silk and GO.

Keywords: commercial silk; graphene oxide; thermal treatment; pressure sensor; motion sensor

1. Introduction

Flexible electronic components have been steadily developed in various fields, including electrically conducting textiles [1–4], thermoelectric textiles [5–7], solar cells [8], secondary batteries [9], and gas sensors [10–12]. Among them, flexible mechanical sensors (strain and pressure sensors) have been of interest because of their utility for sensing human body functions for healthcare, and for use in the Internet of Things (IoT). In particular, textile-based mechanical sensors have the advantage of being lightweight, low-cost, and having superior flexibility [13–16]. Commercial textiles such as cotton, nylon, polyester, and silk have been used as flexible substrates for such sensors. However, other components were used to ensure high sensitivity and flexibility.

Cotton fabric has been decorated with Ag nanowires, Ag flowers, and Ag thread [17–20], and coatings of electrochemically exfoliated graphene film on cotton fabric [21], and coatings of Ag on cotton yarn using Ag paste followed by sintering [22] have been used to provide electrical conductivity. Likewise, electronic textiles for sensors fabricated with nylon and polyester have been achieved using conducting polymer [23], Au and MoS_2-coating [24], graphite-polyurethane (PU) coating on crochet knitted elastic [25], screen-printing of elastic conductive carbon ink on polyester fabric [26], wet-spinning of CNT/thermoplastic PU on silver-plated nylon electrodes [27], coating of CNT/carbon black-PU on the fabric with Ag-coated conductive nylon fiber [28], and spraying of multiwall CNT/TiO_2 conductive suspension on nylon textiles [29]. Mxene has also been introduced to textiles to improve sensitivity [30–34]. In the previous studies mentioned above, complex processes are inevitably required for the fabrication of the sensors.

In the case of silk, C. Wang et al. reported that the wearable strain sensors with carbonized silk fabric had a large gauge factor, but elastic polymer was used due to the thermal instability of

 doi:10.20944/preprints202405.1547.v1

carbonized silk [35]. A pressure sensor was fabricated using Ag nanowires coiled onto silk fiber-wrapped PU [36], and 3D graphene oxide (GO) and a silk fibroin mixture thermally reduced at 700 °C [37]. However, they also involved a complicated procedure and the sensitivity was very low (0.136 ~ 0.54 kPa^{-1}).

Here we report flexible pressure and strain sensors fabricated with reduced GO (rGO)-coated commercial silk (rGOS) fabrics and yarns. The GO was coated by a simple dipping method and then the GO-coated silk (GOS) was thermally reduced at 400 °C. The pressure and strain sensors were prepared by stacking small pieces of rGOS fabrics and twisting rGOS yarns, respectively. The pressure sensor showed superior sensitivity (2.58 ×10^3 kPa^{-1} at low pressure and 1.842 kPa^{-1} at high pressure). The gauge factor (GF) of the strain sensor was relatively low (~ 0.307) but the strain sensor was able to detect human motion (bending) and had good cyclability even after 5000 cycles.

2. Materials and Methods

GO was synthesized with graphite powder (99.995% metals basis, Alfa Aesar) by the modified Hummers method [38]. GO was dissolved in DI water and sonicated for 1.0 h. The GO concentration was 1.0 mg/ml. GO was coated onto the commercial silk fabrics by simply dipping for 30 min and then the GOS fabric was dried at 40 °C in a fume hood. The process was repeated three times to make a uniform coating of GO [2,12]. The GOS fabric was thermally reduced. The rGOS fabrics for the pressure sensors were obtained by thermal treatment at 400 °C for 2.0 hr at a heating rate of 1.0 °C/min in N_2 atmosphere. The rGOS fabrics were cut by 1.0 cm × 1.0 cm and then three pressure sensors were made depending on the number of fabrics. The strain sensors were fabricated by twisting the GOS yarns with an electrically powered drill. After twisting the GOS yarns, the yarns were thermally treated in the same condition.

To observe the morphology of the samples, field emission scanning electron microscopy (FE-SEM, JSM-7800F, JEOL, Japan) was used. The structure of the rGOS was determined by X-ray diffraction (XRD, SmartLab, Rigaku, Tokyo, Japan) with Cu Kα radiation (λ = 1.5418 Å), X-ray photoelectron spectroscopy (XPS, PHI 5000 Versa Probe II, Ulvac-PHI 5000 Versa Probe, Phi(Ø), Chigasaki, Japan), and Raman spectroscopy (Raman-LTPL system, Witec alpha300, Witec, Ulm, Germany) using 532 nm laser. The size of GO was measured by atomic force microscopy (AFM, XE-NSOM, Park Systems, Korea).

3. Results and Discussion

3.1. Structural Investigation

As-synthesized GOs were dispersed in DI water and then they were dropped onto a SiO_2/Si wafer to measure the size of GO by AFM (Figure 1a). The distribution of the lateral size was from 50 nm to 1.95 μm (Figure 1b). The average size of the GOs was 349 nm. Figure 1c,d show optical images of the GOS and rGOS, respectively. After thermal treatment, the dark brown color of the GOS changed to black color (rGOS), and the size of the fabric was reduced. The shrinkage of the fabric was also observed in SEM images of the GOS (Figure 1e) and rGOS (Figure 1f).

The Raman spectroscopy of GOS and rGOS confirmed the existence of GO on silk (the inset of Figure 1e). *D* and *G* peaks were observed in the GO, GOS, and rGOS. The *D* band arises from defects (disorder) and the *G* band is related to C-C stretching of the sp^2 carbon [39]. The *D* peaks were at 1341, 1359, and 1330 cm^{-1} and the *G* peaks were at 1584, 1587, and 1558 cm^{-1} for the GO, GOS, and rGOS, respectively. The peak shifts in the GOS compared with GO are attributed to overlapping with the peaks from the silk. After thermal treatment (rGOS), the *D* and *G* peaks were red-shifted, from 1359 cm^{-1} to 1330 cm^{-1} for the *D* peak and from 1587 cm^{-1} to 1558 cm^{-1} for the *G* peak. This indicates the increase in translational symmetry of the GOS due to the thermal treatment. This behavior was also found in the I_D/I_G ratio. I_D/I_G ratios of the GO, GOS, and rGOS, which were 1.06, 1.06, and 1.01, respectively.

Preprints.org (www.preprints.org) | NOT PEER-REVIEWED | Posted: 23 May 2024 doi:10.20944/preprints202405.1547.v1

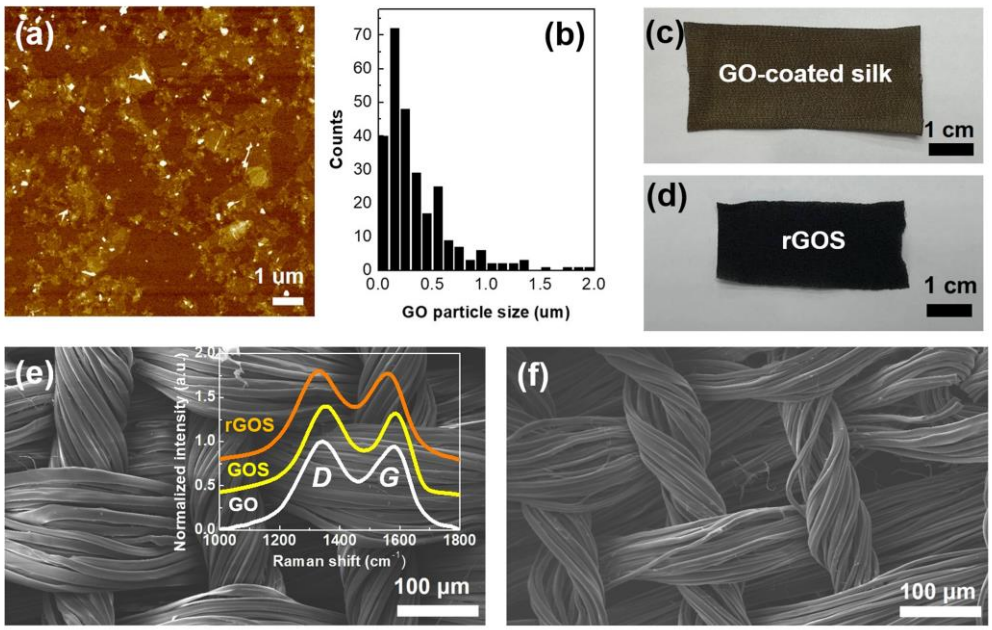

Figure 1. (a) AFM image and (b) the sizes of the GO particles. Optical images of (c) GOS and (d) rGOS fabrics. SEM images of (e) GOS and (f) rGOS fabrics. The inset in (e) shows the Raman D and G peaks of GO, GOS, and rGOS.

Figure 2a displays the normalized XRD patterns of the GO sheet, GOS, and rGOS. The peak at 11.44° ((001) plane) of the GO sheet indicates that the interlayer distance of the GO is 7.732 Å. The XRD patterns of the GOS were similar to those of pristine silk [40]. After heat treatment, the peak for the (002) lattice plane at 22.95° appeared in the rGOS. The relatively broad peak for the (002) plane originated from the overlapping of various amorphous structures. [41].

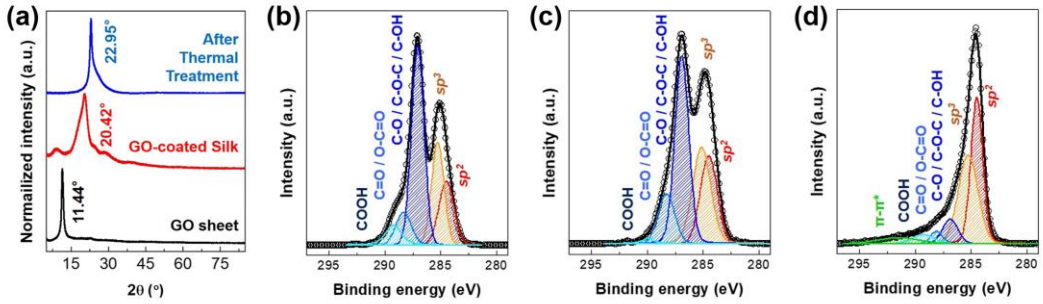

Figure 2. (a) XRD patterns of the GO, GOS, and rGOS. XPS C1s peaks of (b) GO, (c) GOS, and (d) rGOS. A decrease in the oxygen functional groups was observed in the rGOS.

The decrease in oxygen functional groups due to thermal treatment was investigated using the XPS C1s peak (Figures 2b–d). A large amount of oxygen functional groups (COOH, C=O/O-C=O, C-O/C-O-C/C-OH) was clearly observed in the GO sheet (Figure 2b) and GOS (Figure 2c). In contrast, the functional groups significantly decreased in rGOS (Figure 2d). At the O1s peak, the amount of O-H, C-O, and C=O species in the GOS was similar to that of the GO sheet but C-O bonds decreased in the rGOC (Figures S1a–c). The nitrogen from the silk was found in the N1s peak of the GOS and rGOS (Figures S1d–f). Interestingly, pyridinic-N developed after thermal treatment, resulting from carbonized silk. The XRD, Raman spectroscopy, and XPS studies showed the reduction of GO and the carbonization of silk, which endow electrical conductivity to rGOS.

 doi:10.20944/preprints202405.1547.v1

3.2. Pressure Sensors

Figure 3a is a side view of a single rGOS fabric. The average thickness is 349.6 μm. The flexible pressure sensors were made very simply with the rGOS fabrics. First, the fabric was cut into a square, whose length on a side was 1.0 cm. Next, the cut fabrics were stacked between Al plates (Figure 3f). We chose 3, 5, and 7 layers of fabric. The thickness of the 7-layer pressure sensor was about 4.52 mm (Figure 3b).

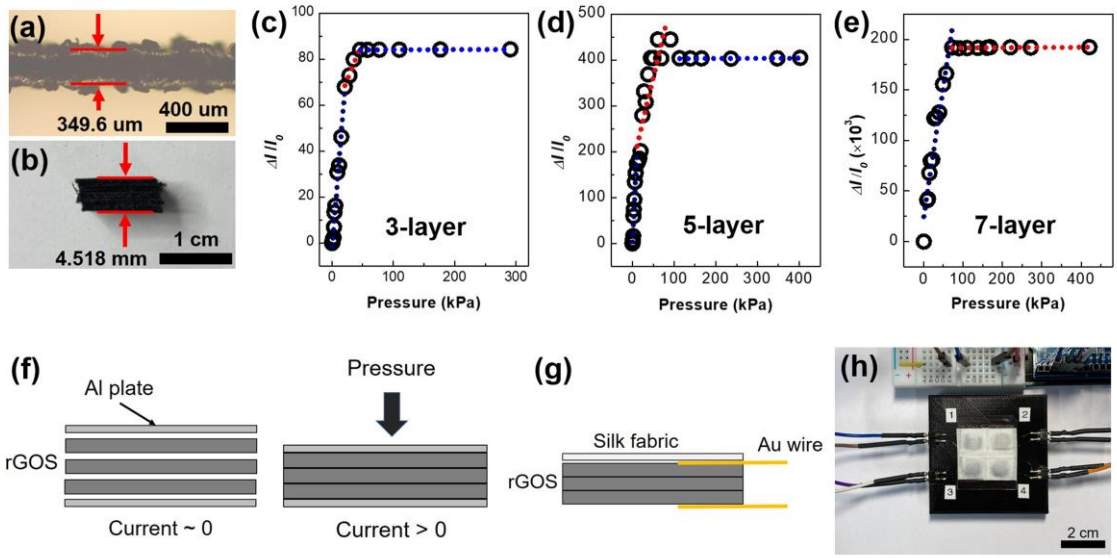

Figure 3. A side-view of (a) a single rGOS fabric and (b) a 7-layer rGOS fabric. The sensitivities of the rGOS pressure sensors fabricated with (c) 3-layer, (d) 5-layer, and (e) 7-layer of the fabrics. (f) The operating mechanism of the pressure sensor. (g) The scheme of the textile-based pressure sensor module and (f) optical image of the two-by-two pressure sensor module.

The sensitivity of the three sensors is depicted in Figures 3c-e. The sensitivity of the 3-layer pressure sensor was 3.32 kPa^{-1} at low pressures (0.5 - 21 kPa), 0.662 kPa^{-1} at 21 – 46 kPa, and 0.665 $\times 10^{-3}$ kPa^{-1} at high pressures (46 – 290 kPa) (Figure 3c). For the 5-layer pressure sensor, the sensitivity was 18.7 kPa^{-1} at low pressures (0.4 – 10.9 kPa), 3.82 kPa^{-1} at 10.9 – 91.3 kPa, and 2.57 $\times 10^{-3}$ kPa^{-1} at high pressures (91.3 – 402.1 kPa) (Figure 3d). Interestingly, an enormous increase in sensitivity was measured in the 7-layer pressure sensor. The sensitivities were 2.58 $\times 10^{3}$ kPa^{-1} at low pressures (0.2 – 72.3 kPa) and 1.84 kPa^{-1} at high pressure (72.3 – 421 kPa) (Figure 3e). To the best of our knowledge, the sensitivity at low pressure of the 7-layer sensor is the best among the textile-based sensors except for the pressure sensor fabricated with Ag nanowire (AgNW)-coated cotton fabric [17] (Table 1). The operation of the sensor is shown in Figure 3f. Without pressure the resistance (R) of the sensor was large because the rGOS layers barely contacted each other. The R significantly decreased as soon as pressure was applied, due to the electrical contact between the layers. The number of layer-dependent sensitivity was determined by the initial R of the sensors. The increase in the layer number increased the initial R. For example, the resistances of the 3-layer and 7-layer sensors were 0.42 MΩ and 958 MΩ, respectively.

 doi:10.20944/preprints202405.1547.v1

Table 1. Comparison of characteristics of the pressure sensors.

Textile	Materials/methods	Sensitivity (kPa^{-1})	Ref.
Silk	Silkworm cocoon, GO, $C_6H_{12}O_6$, NaOH/hydrothermal and freeze-drying	0.54 ~ 0.21	37
Silk	Silkworm fiber, AgNW, PU, CNT/Coiling AgNW onto silk fiber-wrapped PU yarn	0.136	36
Cotton	Cotton fabric, polyester, Kapton tape, sodium dodecylbenzene sulfonate, VHB film, CNT, Ni/CNT-coating on cotton fabric by dipping, patterning using CO_2 laser scribing, Ni-coating with the aid of the mask via electroless plating,	14.4	43
Cotton	Cotton fabric, AgNW, $FeCl_3$, ethylene glycol, poly(vinylpyrrolidone), Ag paste/Synthesis of AgNW using a hydrothermal method, Fabrication of Ag paste on the cotton fabric by screen printing process, AgNW coating on a cotton by soaking process	4.42×10^3, (Comparable to the results in this study)	18
Cotton	Cotton fabric, AgNW, isopropyl alcohol, polyvinyl pyrrolidone, ethylene glycol, $AgNO_3$, NaCl/Synthesis of AgNW using hydrothermal method, AgNW coating on a cotton by dipping	2.16×10^4	17
Cotton	Knitted cotton/spandex fabric (KSCF), pyrrole, ferric chloride hexahydrate, sodium 5-sulfosalicylate, cyclohexane, $AgNO_3$, sodium citrate, KNO_3, Na_2SO_4/Synthesis of PPy@KSCF using in situ polymerization method, preparation of PPy@KSCF with Ag flower using an electrodeposition process	17.41	19
Cotton	Cotton, graphite, stainless steel, PDMS, $(NH_4)_2SO_4$, NMP, NaOH/ Electrochemically exfoliation of graphene (EEG), Coating of EEG films on cotton using a hot press	0.16	21
Nylon, cotton, silk	Nylon, cotton, silk, PU filament/Ag coating on nylon yarn by ion plating method, wrapping of cotton yarn around PU filament and silk around Ag-coated nylon yarn using covering machine	0.01884	42
Polyester	Polyester, MoS_2, $HAuCl_4$, ethanol/Treatment of the fiber with air plasma, MoS_2 coating by dropping, immersing of the fiber in an aqueous $HAuCl_4$ to grow Au nanostructure	0.19	24
Polyester	Polyester fabric, carbon ink, waterborne PU (WPU), CNT, Venetian fabric, CNT paste/Coating of carbon ink on polyester by screen-printing and curing at 100 °C, mixture of cationic WPU and anionic WPU with CNT suspension,	3.42	26

 doi:10.20944/preprints202405.1547.v1

	Electrostatic deposition of WPU/CNT by dipping of Venetian fabric into WPU/CNT suspensions		
Silk	GO, commercial silk/GO coating on silk by dipping method, thermal treatment at 400 °C to reduce GO	2.58 ×10^3	This work

With these results, we fabricated a two-by-two pressure module with the rGOS fabrics (0.5 × 0.5 cm^2) and Au wires. The surface of the module was protected with pristine silk fabric (Figures 3g and 3h). The module directly measured the applied force, indicated by different colors with the Labview program (Figure S2). Figure 4 displays the measurement of the pressures of the four sensors in the module. The numbers in the red and white boxes indicate the applied forces. The response time of the sensors was 300 ms (Figure S3).

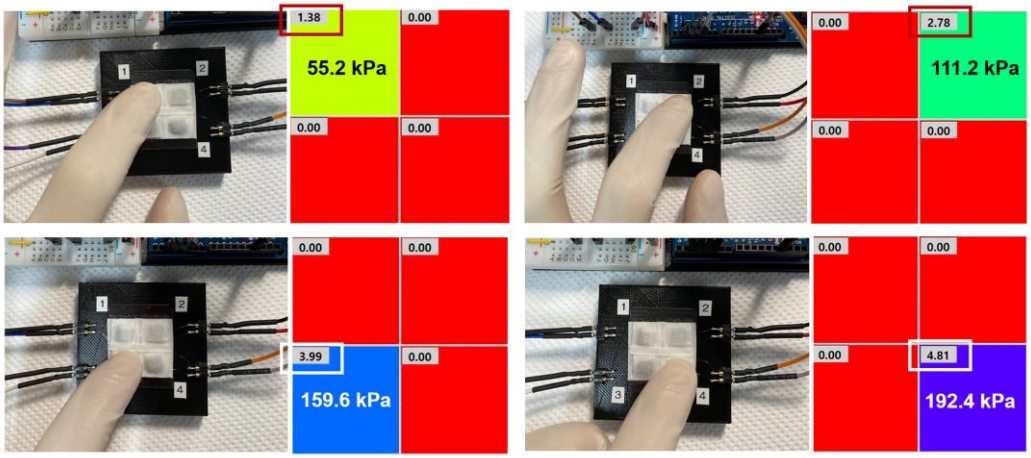

Figure 4. Real-time pressure sensing of each sensor in the module with the Labview program.

3.3. Motion Sensors

The strain sensors were fabricated with GOS yarns. First, the GO-coated yarn was twisted using an electrically powered drill (Figure 5a). Figure 5b shows the variation in force while twisting the yarn. Before being twisted, the force was unstable but the force was relatively stable after twisting began (yellow box). Then, the twisted GOS yarn was thermally treated using the same condition as that for fabricating the rGOS fabric. Evenly twisted yarn was found in the SEM image (Figure 5c).

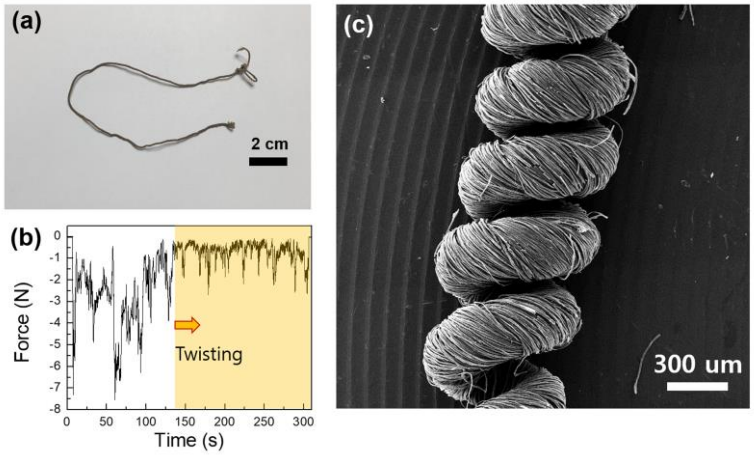

Figure 5. (a) Optical image of the twisted rGOS yarn. (b) The variation in force during twisting of the yarn. (c) SEM image of the twisted rGOS yarn.

 doi:10.20944/preprints202405.1547.v1

Figure 6 depicts the strain-dependent *R*. As the twisted yarn was stretched from 4.40 cm (L0) to 7.15 cm (162.5%) (Figure 6a), the *R* changed from 2.295 MΩ (R0) to 1.855 MΩ (Figure 6b). The decrease in R can be explained by the increase in the electrically conducting paths because the rGOS fibers in the yarn contacted each other when the yarn was stretched. Although the *R* slightly increased (*R* = 2.308 MΩ, see the red triangle in Figure 6), *R* almost recovered when the strain sensor was released again. The increase in *R* was caused by breaking some parts of the fibers when the yarn was stretched to its maximum, as shown in Figure S4. The variation in *R* was 19.17% at 162.5% of stretching. The GF is defined by $(\Delta RL_0)/(R_0\Delta L)$. The GF of the strain sensor was small (GF = 0.307) compared with previous studies [25,29,33,35] but it was larger than the cotton yarn with Ag-paste [22] and Ag-coated nylon [42]. Hence, we found that the twisted rGOC yarn could be used as a motion sensor.

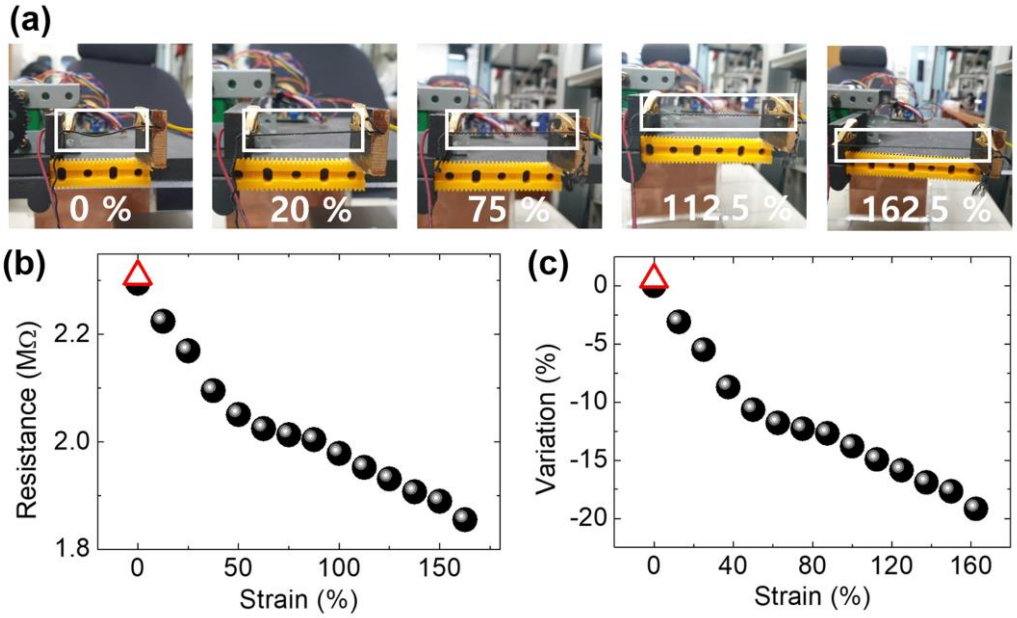

Figure 6. (a) Optical images when applying strain to the twisted rGOS yarn (white boxes). The yarn was maximally stretched to 162.5%. (b) The strain-dependent R and (c) $\Delta R/R_0$ (variation), here $\Delta R = R - R_0$ and R_0 is the initial R (when the strain is zero). The negative value means that the R decreased as the strain increased.

Figure 7 shows the detection of finger motion. The twisted rGOS yarn was attached to a Latex glove with Ag foil to monitor the motion of the finger (Figure 7a). The current was approximately 240 nA when the finger was spread out. As the finger was bent about 90°, the current increased to ~ 280 nA. The change in the current was about 16.7% (Figure 7b). This indicates that the twisted rGOS yarns functioned as a motion sensor. To check the cyclability for bending, we made a hand using 3D printing with a motor (Figure 7c and Figure S5). The variation in current (the ratio, $\Delta I/I_0$, I_0 is the current corresponding to stretching and $\Delta I = I - I_0$) for bending and stretching was stable for 5000 cycles (Figure 7d). Figures 7e and 7f display variations in current near 2500 cycles and 5000 cycles, respectively. This indicates the good cyclability of the motion sensor even after 5000 cycles. The difference in current variation between the human finger (16.7%) and the artificial finger (~3.5%) was due to the bending degree. The human finger was bent 90° but the artificial hand could only be bent to a maximum of about 45°. The double peaks during bending were caused by two finger joints, as shown in Figure 7c (white circles).

 doi:10.20944/preprints202405.1547.v1

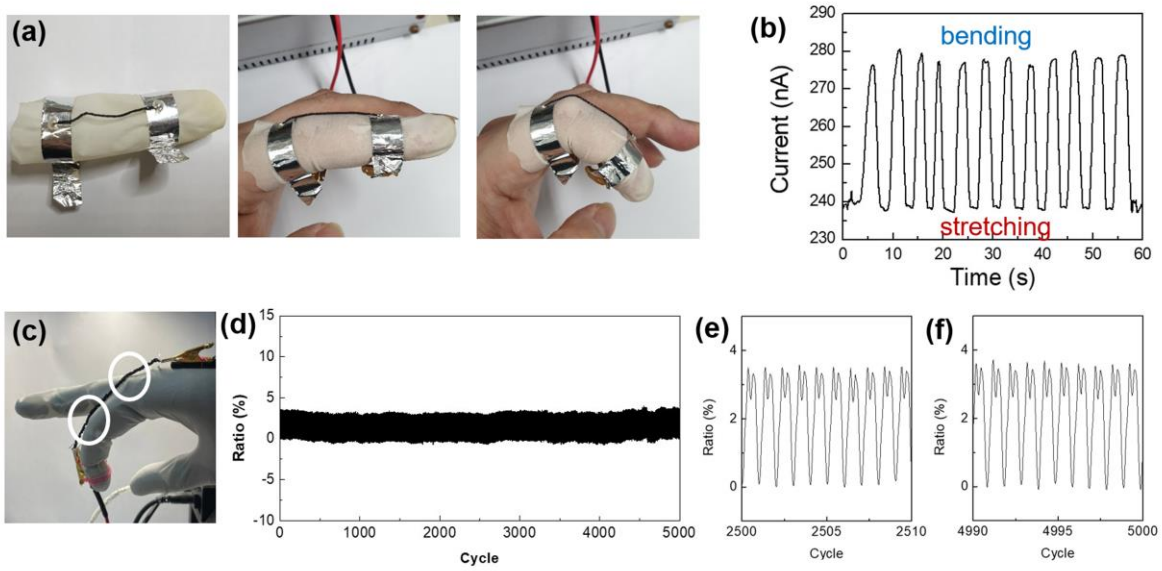

Figure 7. (a) Test of the motion sensor with a human finger and (b) its result. The current increases as the finger is bent. (c) An artificial hand fabricated using a 3D printer. (d) Cyclability of the yarn during 5000 cycles and near (e) 2500 cycles and (f) 5000 cycles.

4. Conclusions

In summary, we fabricated flexible pressure and motion sensors with GO and commercial silk fabric and yarns, respectively. The sensors were simply produced by dipping the silk into the GO solution followed by thermal treatment. The pressure sensors were achieved by stacking the rGOS fabrics. The sensitivity of the 7-layer pressure sensor was 2578 kPa^{-1}. As shown in Table 1, this value is very large compared to other flexible pressure sensors. The GF of the motion sensors obtained from the twisted rGOS yarns was 0.307. The motion sensors successfully detected the bending of a finger, and the response for bending and stretching was stable up to 5000 cycles. This study provides the possibility to synthesize ultrasensitive pressure and motion sensors without complicated procedures.

Supplementary Materials: The following supporting information can be downloaded at the website of this paper posted on Preprints.org. Figure S1: O1s and N1s XPS spectra; Figure S2: pressure sensor with Labview program; Figure S3: response time of the pressure sensor; Figure S4: SEM image of twisted rGOS yarn stretched maximally; Figure S5: home-made artificial hand.

Author Contributions: Conceptualization, K. H. L., and B. H. K.; methodology, H.-S. J. and B. H. K.; software, H.-S. J. and K. H. L.; validation, H.-S. J., K. H. L., and B. H. K.; formal analysis, H.-S. J., K. H. L., and B. H. K.; investigation, H.-S. J., K. H. L., and B. H. K.; data curation, H.-S. J., K. H. L., and B. H. K.; writing—original draft preparation, K. H. L. and B. H. K.; writing—review and editing, K. H. L. and B. H. K.; visualization, H.-S. J., K. H. L., and B. H. K.; supervision, K. H. L. and B. H. K. All authors have read and agreed to the published version of the manuscript.

Funding: This work was supported by the National Research Foundation of Korea (NRF) by the Korea Government (MSIT) (NRF-2020R1A2C4001513).

Data Availability Statement: Data are contained within the article.

Acknowledgments: The authors thank W. T. Jung and J. W. Jeon for contributing to some parts of the experiments.

Conflicts of Interest: The authors declare no conflicts of interest.

References

1. Yun, Y. J.; Hong, W. G.; Kim, W.-J.; Jun, Y.; Kim, B. H. A novel method for applying reduced graphene oxide directly to electronic textiles from yarns to fabrics. *Adv. Mater*. **2013**, *25*, 5701-5705.
2. Jeon, J. W.; Cho, S. Y.; Jeong, Y. J.; Shin, D. S., Kim, N. R.; Yun, Y. S.; Kim, H.-T.; Choi, S. B.; Hong, W. G.; Kim, H. J.; et al. Pyroprotein-based electronic textiles with high stability. *Adv. Mater*. **2017**, *29*, 1605479.
3. Jeon, J. W.; Oh, J. Y.; Cho, S. Y.; Lee, S.; Jang, H.-S.; Jung, W. T.; Kim, J.-G.; Kim, H.; Kim, H. J.; Kim, S. Y.; et al. Pyroprotein-based electronic textiles with high thermal durability. *Mater. Today* **2018**, *21*, 944-950.
4. Jang, H.-S.; Kim, S.; Park, I.; Jung, W. T.; Seo, J. H.; Kwon, J.-H.; Hong, W. G.; Mrówczyński, R.; Lee, H.; Choi, S. B.; et al. Long-range ordered graphitic structure in silk fibers delaminated using dopamine and thermal treatment for super-flexible electronic textiles: Possible applications for magnetic and thermoelectric textiles. *Adv. Compos. Hybrid Mater*. **2024**, *7*, 37.
5. Zhang, L.; Shi, X.-L.; Yang, Y.-L.; Chen, Z.-G. Flexible thermoelectric materials and devices: From materials to applications. *Mater. Today* **2021**, *46*, 62-108.
6. Li, X.; Cai, K.; Gao, M.; Du, Y.; Shen, S. Recent advances in flexible thermoelectric films and devices. *Nano Energy* **2021**, *89*, 106309.
7. Cao, T.; Shi, X.-L.; Chen, Z.-G. Advances in the design and assembly of flexible thermoelectric device. *Prog. Mater. Sci*. **2023**, *131*, 101003.
8. Liu, W.; Liu, Y.; Yang, Z.; Xu, C.; Li, X.; Huang, S.; Shi, J.; Du, J.; Han, A.; Yang, Y.; et al. Flexible solar cells based on foldable silicon wafers with blunted edges. *Nature* **2023**, *617*, 717-723.
9. Yeon, J. S.; Park, S. K.; Kim, S.; Jang, G.; Bae, J.; Jang, H.-S.; Kim, B. H.; Kim, Y.; Park, H. S. Self-supported VO_2 on polydopamine-derived pyroprotein-based fibers for ultrastable and flexible aqueous zinc-ion batteries. *Carbon Energy* **2024**, e469.
10. Ou, L.-X.; Liu, M.-Y.; Zhu, L.-Y.; Zhang, D. W.; Lu, H.-L. Recent progress on flexible room-temperature gas sensors based on metal oxide semiconductor. *Nano-Micro Lett*. **2022**, *14*, 206.
11. Kim, J.-H.; Mirzaei, A.; Kim, H. W.; Kim, S. S. Flexible and low power CO gas sensor with Au-functionalized 2D WS_2 nanoflakes. *Sens. Actuators B: Chem*. **2020**, *313*, 128040.
12. Jung, W. T.; Jeon, J. W.; Jang, H.-S.; Kim, D. Y.; Lee, H.-K.; Kim, B. H.; Commercial silk-based electronic textiles for NO_2 gas sensing. *Sens. Actuators B: Chem*. **2020**, *307*, 127596.
13. Chen, G.; Xiao, X.; Zhao, X.; Tat, T.; Bick, M.; Chen, J. Electronic textiles for wearable point-of-care systems. *Chem. Rev*. **2022**, *122*, 3259-3291.
14. Liu, X.; Miao, J.; Fan, Q.; Zhang, W.; Zuo, X.; Tian, M.; Zhu, S.; Zhang, X.; Qu, L. Recent progress on smart fiber and textile based wearable strain sensors: materials, fabrications and applications. *Adv. Fiber Mater*. **2022**, *4*, 361-389.
15. Zhang, J.-w.; Zhang, Y.; Li, Y.-y.; Wang, P. Textile-based flexible pressure sensors: A review. *Polym. Rev*. **2022**, *62*, 65-94.
16. Chen, J.; He, T.; Du, Z.; Lee, C. Review of textile-based wearable electronics: From the structure of the multi-level hierarchy textiles. *Nano Energy* **2023**, *117*, 108898.
17. Lian, Y.; Yu, H.; Wang, M.; Yang, X.; Li, Z.; Yang, F.; Wang, Y.; Tai, H.; Liao, Y.; Wu, J.; et al. A multifunctional wearable E-textile via integrated nanowire-coated fabrics. *J. Mater. Chem. C* **2020**, *8*, 8399-8409.
18. Lai, C.; Wu, X.; Huang, C.; Yuan, X.; Liang, H.; Wang, S.; Lin, K.; Wang, Y. Fabrication and performance of full textile-based flexible piezoresistive pressure sensor. *J. Mater. Sci: Mater. Electron* **2022**, *33*, 4755-4763.
19. Lv, J.; Liu, Z.; Zhang, L.; Li, K.; Zhang, S.; Xu, H.; Mao, Z.; Zhang, H.; Chen, J.; Pan, G. Multifunctional polypyrrole and rose-like silver flower-decorated E-textile with outstanding pressure/strain sensing and energy storage performance. *Chem. Eng. J*. **2022**, *427*, 130823.
20. Honda, S.; Zhu, Q.; Satoh, S.; Arie, T.; Akita, S.; Takei, K. Textile-based flexible tactile force sensor sheet. *Adv. Funct. Mater*. **2019**, *29*, 1807957.
21. Kim, Y.; Park, J. B.; Kwon, Y. J.; Hong, J.-Y.; Jeon, Y.-P.; Lee, J. U. Fabrication of highly conductive graphene/textile hybrid electrodes via hot pressing and their application as piezoresistive pressure sensors. *J. Mater. Chem. C* **2022**, *10*, 9364-9376.
22. Li, X.; Li, X.; Wang, M.; Zheng, R.; Jin, Y.; Gu, Z. Flexible and strain conductive cotton yarn enabled by low-temperature sintering of silver paste with multifunctional sensing capability in human motion detection and wearable applications. *Chem. Eng. J*. **2023**, *471*, 144843.
23. Lim, S. J.; Bae, J. H.; Jang, S. J.; Lim, J. Y.; Ko, J. H. Development of textile-based pressure sensor and its application. *Fibers Polym*. **2018**, *19*, 2622-2630.
24. Lan, L.; Zhao, F.; Yao, Y.; Ping, J.; Ying, Y. One-step and spontaneous in situ growth of popcorn-like nanostructures on stretchable double-twisted fiber for ultrasensitive textile pressure sensor. *ACS Appl. Mater. Interfaces* **2020**, *12*, 10689-10696.
25. Alam, T.; Saidane, F.; al Faisal, A.; Khan, A.; Hossain, G. Smart-textile strain sensor for human joint monitoring. *Sens. Actuators A: Phys*. **2022**, *341*, 113587.

26. Liu, Q.; Zhang, Y.; Sun, X.; Liang, C.; Han, Y.; Wu, X.; Wang, Z. All textile-based robust pressure sensors for smart garments. *Chem. Eng. J*. **2023**, *454*, 140302.
27. Zhong, W.; Ming, X.; Jiang, H.; Ke, Y.; Ding, X.; Li, M.; Jia, K.; Wang, D. Full-textile human motion detection systems integrated by facile weaving with hierarchical core-shell piezoresistive yarns. *ACS Appl. Mater. Interfaces* **2021**, *13*, 52901-52911.
28. Zhu, H.; Dai, S.; Cao, J.; Bai, H.; Zhong, Y.; Zhang, Z.; Cheng, G.; Yuan, N.; Ding, J. A high-performance textile pressure sensor based on carbon black/carbon nanotube-polyurethane coated fabrics with porous structure for monitoring human motion. *Mater. Today Commun*. **2022**, *33*, 104541.
29. Ma, J.; Qing, Y.; Song, H.; Yao, Y.; Xu, X.; Long, C.; Liu, N.; Li, H.; Liu, C. Micro-/nanofiber-coupled superhydrophobic and conductive textile for underwater wearable strain sensors with full-scale human motion detection ability. *J. Mater. Chem. C* **2023**, *11*, 9539-9551.
30. He, W.; Sohn, M.; Ma, R.; Kang, D. K. Flexible single-electrode triboelectric nanogenerators with MXene/PDMS composite film for biomechanical motion sensors. *Nano Energy* **2020**, *78*,105383.
31. Zhen, X.; Wang, P.; Zhang, X.; Hu, Q.; Wang, Z.; Nie, W.; Zou, L.; Li, C.; Han, X. Breathable, durable and bark-shaped MXene/textiles for high-performance wearable pressure sensors, EMI shielding and heat physiotherapy. *Compos. Part A* **2022**, *152*, 106700.
32. Meena, J. S.; Choi, S. B.; Khanh, T. D.; Shin, H. S.; Choi, J. S.; Joo, J.; Kim, J.-W. Highly stretchable and robust textile-based capacitive mechanical sensor for human motion detection. *Appl. Surf. Sci*. **2023**, *613*, 155961.
33. Ma, J.; Qing, Y.; Song, H.; Cheng, X.; Li, Z.; Long, C.; Liu, C. Synergistically coupled double conductive coating-based electronic textiles with superhydrophobic and high-performance strain sensing properties for underwater human motion sensing applications. *Chem. Eng. J*. **2023**, *471*, 144284.
34. Yao, D.; Tang, Z.; Liang, Z.; Zhang, L.; Sun, O.-J.; Fan, J.; Zhong, G.; Liu, Q.-X.; Jiang, Y.-P.; Tang, X.-G.; et al. Adhesive, multifunctional, and wearable electronics based on MXene-coated textile for personal heating systems, electromagnetic interference shielding, and pressure sensing. *J. Colloid Interf. Sci*. **2023**, *630*, 23-33.
35. Wang, C.; Li, X.; Gao, E.; Jian, M.; Xia, K.; Wang, Q.; Xu, Z.; Ren, T.; Zhang, Y. Carbonized silk fabric for ultrastretchable, highly sensitive, and wearable strain sensors. *Adv. Mater*. **2016**, *28*, 6640-6648.
36. Wu, R.; Ma, L.; Hou, C.; Meng, Z.; Guo, W.; Yu, W.; Yu, R.; Hu, F.; Liu, X. Y. Silk composite electronic textile sensor for high space precision 2D combo temperature-pressure sensing. *Small* **2019**, *15*, 1901558.
37. Ma, X.; Kong, Z.; Gao, Y.; Bai, Y.; Wang, W.; Tan, H.; Cai, Z.; Cai, J. Anisotropic free-standing aerogels based on graphene/silk for pressure sensing and efficient adsorption. *ACS Appl. Mater. Interfaces* **2023**, *15*, 30630-30642.
38. Chen, J.; Yao, B.; Li, C.; Shi, G. An improved Hummers method for eco-friendly synthesis of graphene oxide. *Carbon* **2013**, *64*, 225-229.
39. Rerumbilavil, S.; Sankar, P.; Rose, T. P.; Philip, R. White light Z-scan measurements of ultrafast optical nonlinearity in reduced graphene oxide nanosheets in the 400-700 nm region. *Appl. Phys. Lett*. **2015**, *107*, 051104.
40. Jang, H.-S.; Jung, W. T.; Chung, C.; Kim, M.; So, Y.; Song, S.; Kim, B. H. Charge transport at the interface between graphene oxide and silk in highly flexible commercial silk-based e-textile treated at high temperatures. *ACS Appl. Electron. Mater.* **2022**, *4*, 3543-3548.
41. Jung, W. T.; Jang, H.-S.; Jeon, J. W.; Kim, B. H. Effect of oxygen functional groups in reduced graphene oxide-coated silk electronic textiles for enhancement of NO_2 gas-sensing performance. *ACS Omega* **2021**, *6*, 27080-27088.
42. Si, S.; Sun, C.; Qiu J.; Liu, J.; Yang J. Knitting integral conformal all-textile strain sensor with commercial apparel characteristics for smart textiles. *Appl. Mater. Today* **2022**, *27*, 101508.
43. Liu, M.; Pu, X.; Jiang, D.; Liu, T.; Huang, X.; Chen, L.; Du, C.; Sun, J.; Hu, W.; Wang, Z. L. Large-area all-textile pressure sensors for monitoring human motion and physiological signals. *Adv. Mater*. **2017**, *29*, 1703700.